Available online at www.sciencedirect.com

jmr&t Journal of Materials Research and Technology

www.jmrt.com.br

Original Article

Influence of microstructure of carbon fibre reinforced polymer on the metal in contact

Chi Zhang[a], Dajiang Zheng[a], Guang-Ling Song[a,*], Yang Guo[b], Ming Liu[b], Hamid Kia[c]

[a] Centre for Marine Materials Corrosion and Protection, State Key Laboratory of Physical Chemistry of Solid Surfaces, College of Materials, Xiamen University, 422 S. Siming Rd., Xiamen 361005, China

[b] China Science Lab, GM Global R&D, 56 Jinwan Road, Shanghai, China

[c] Chemicals and Materials Science Lab, GM Global R&D, 30500 Mound Road, Warren, USA

ARTICLE INFO

Article history:
Received 5 March 2019
Accepted 31 October 2019
Available online 20 November 2019

Keywords:
Carbon fibre reinforced polymer (CFRP)
Composite
EIS
Galvanic corrosion
Defect

ABSTRACT

The influence of the microstructure of carbon fibre reinforced polymers (CFRPs) with epoxy matrix (E-CFRP) and nylon matrix (T-CFRP) on the galvanic behaviour of DP590 steel, 6022-aluminium alloy, 1040-steel and AZ31-magnesium alloy was investigated in the GMW14872 solution. The E-CFRP/metal couples were initially more galvanic corrosion resistant, but their galvanic corrosion gradually became more severe than the T-CFRP/metal couples. The effective micro-defects in the surface polymer layer of the CFRP samples critically determined the galvanic corrosion. A detailed surface layer model was proposed, the electrochemical processes through the surface polymer layers during galvanic corrosion were discussed. A better understanding on the microstructure of CFRP determined by composites manufacture process can be obtained.

1. Introduction

Due to their high strength, high modulus, high corrosion resistance and especially light weight, carbon fibre reinforced polymers (CFRP) have been regarded as a promising material to replace some traditional high strength metals. For example, the use of CFRPs in car body can lead to obvious weight reduction, improved mileage, and eventually reduced carbon dioxide emission [1]. The high strength and corrosion resistance [2–4] have also made CFRPs one of the durable materials in infrastructure, such as the highways, oil and gas production facilities, chemical refineries, water and wastewater treatment systems. They have even been successfully used to strengthen the elements of concrete bridge structures [5]. However, because of the high fabrication cost, most important applications of CFRPs today are mainly limited to military and aerospace industries [6,7]. There is no doubt that CFRPs will find more applications in various industries after they become affordable.

Currently, CFRPs are usually used together with metallic engineering materials, such as steels and aluminium alloys.

* Corresponding author.
E-mails: Guangling.song@hotmail.com, glsong@xmu.edu.cn (G. Song).
https://doi.org/10.1016/j.jmrt.2019.10.085

Since carbon fibre is a good electronic conductor like a metal [8], many electrochemical reactions can occur on its surface. When a CFRP is in contact with a metal, there will be a galvanic process between the CFRP and metal, which can cause corrosion damage to the anodic metal. This is always a major concern in practical applications of CFRPs [9–16].

There have been quite a few publications on the galvanic corrosion of metals in contact with CFRPs [9,13,17–25]. Compared with the damage of the anode metals, the detailed role of the cathode CFRP in the galvanic corrosion has appeared to be overlooked. Currently, investigations into the effect of CFRP microstructure on the galvanic process are very rare, and the limited research on CFRPs is mainly focused on their mechanical properties, while their electrochemical performance, especially their galvanic effect, is seldom studied, let alone the possible damage of the CFRPs themselves resulting from the galvanic effect [26].

In fact, the microstructure of a CFRP, particularly the surface polymer layer, can significantly affect the electrochemical behaviour of the CFRP and strong electrochemical reactions on the CFRP can even damage its surface polymer layer [27]. These findings imply that the microstructure of a CFRP has a significant effect on the galvanic behaviour of a metal in contact, and the galvanic reaction may in return lead to degradation of the CFRP. These implications closely concern practical applications of CFRPs, but they have unfortunately not been systematically investigated so far. A study on the interaction between cathode CFRP degradation and anode metal corrosion will not only deepen the fundamental understanding of traditional galvanic theory, but also provide a guide for CFRP/metal joint design in industries.

In this study, the basic electrochemical properties of metals and the coupled CFRPs with different composite microstructures, surface polymer layers and matrices were measured to understand the galvanic processes between the anode metals and the cathode CFRPs. A surface polymer layer model was proposed to interpret the effect of the CFRP microstructure on the galvanic corrosion behaviour of the coupled metal anode.

2. Experimental

2.1. Materials and solution

Two types of CFRPs, E-CFRP and T-CFRP, as well as Zn-coated DP590 steel, 1040-steel, 6022-aluminium alloy and AZ31-magnesium alloy were used in this study. All the samples had dimensions of 100 mm × 40 mm × 1.6 mm. Their chemical compositions and constitutions are shown in Table 1.

All the materials were cleaned with ethanol and distilled water and then dried in flowing air. The surface polymer layers of some of the CFRPs were also removed by abrading to expose their carbon fibre bundles. The arrangements of the carbon fibre bundles in these two types of CFRPs are quite different [8]; the E-CFRP contains 8 carbon fibre layers in different directions at **0/45/−45/90/90/−45/45/0**°, respectively, while the T-CFRP contains 6 carbon fibre layers, and in each layer the fibre bundles cross vertically together like the texture of a "woven bag" [27].

Considering the possible application of these CFRPs in the auto industry, a GM standard test solution containing 0.9 wt% NaCl + 0.1 wt% $CaCl_2$ + 0.075 wt% $NaHCO_3$ (GM WORLDWIDE ENGINEERING STANDARD-GMW14872) was used in this study.

2.2. Electrochemical measurements

A three-electrode conventional electrolyte cell and an electrochemical measurement system AUTOLAB (Metrohm) were used to measure the open-circuit potentials (OCP), electrochemical impedance spectroscopy (EIS) spectra and polarization curves of the metals and CFRPs. In the cell, a platinum plate was used as the counter electrode and an Ag/AgCl/saturated KCl electrode as the reference. The surface area of the tested sample for measurement was around 0.78 cm^2. In polarization curve measurements, the potentiodynamic scanning rate was 1 mV/s. The EIS spectra of the metal samples were measured at different immersion times at their OCPs, and those of the CFRPs at their OCPs, −1 V (vs OCP) and +1 V (vs OCP). In all the EIS measurements, the AC potential amplitude was 10 mV, and the frequency range was from 0.1 Hz to 100 kHz with 10 frequency points per logarithmic decade.

The galvanic currents I_gs between CFRP samples and metals were measured in a different electrolyte cell as shown in Fig. 1, in which W1 represented the CFRP sample (a E-CFRP or T-CFRP coupon), W2 was a metal sample, and RE was an Ag/AgCl reference electrode. They were connected to an electrochemical measurement system P4000+ (AMETEK). The distance between W1 and W2 was 6 cm, the exposed areas of the CFRP and metal samples in the solution were around 0.78 cm^2, and the electrolyte volume in the cell was 100 ml. The measurement lasted 8 h for each galvanic couple.

2.3. Morphology characterization

The surface morphologies of the samples after galvanic corrosion tests were observed and recorded by an optical microscope, Leica DMV6. The layer structure of CFRP was observed by SEM, TM-3000.

3. Results

3.1. Cross-section microstructure of CFRP

The difference of layer structure between E-CFRP and T-CFRP are shown in Fig. 2. There are obviously many "gaps" between carbon fibre and polymer matrix in E-CFRP (see Fig. 2a). Those kind of "gaps" never occur on the cross-section of T-CFRP (see Fig. 2b), meaning E-CFRP have much more interspace than T-CFRP in the inner structure.

3.2. Open circuit potentials

The open circuit potentials (OCPs), denoted as Es in this paper, of all the tested samples in the GMW-14872 solution are shown in Fig. 3. The OCPs of the CFRPs were more positive than those of the metals, because the electrochemical behaviour of carbon fibre in CFRP was similar to a noble metal like gold or

Table 1 – Chemical compositions of the test metals and the constitutions of the composite materials.

Sample	Composition and constitution
E-CFRP	Fabricated in GM R&D containing 57 vol.% carbon fibre in epoxy
T-CFRP	Bond Laminates TEPEX Dynalite 201-C200(6) containing 45 vol.% carbon fibre in nylon 6, 6 (200 g/m^2 fabric, 6 layers)
DP590 steel	Fe (Bal.), C (0.095 wt%), Cr (0.03 wt%), Ni (0.035 wt%), Si (0.31 wt%); Mn (1.75 wt%), Ti (0.002 wt%), P (0.011 wt%), S (0.005 wt%); Zn coating on the surfaces
1040-steel	Fe (Bal.), C (0.37–0.45 wt%), Si (0.17–0.37 wt%), Mn (0.5–0.8 wt%), S (≤0.035 wt%), P (≤0.035 wt%), Cr (≤0.25 wt%), Ni (≤0.25 wt%), Cu (≤0.25 wt%)
6022 Al alloy	Al (Bal.), Si (0.8–1.5 wt%), Fe (0.05–0.2 wt%), Cu (0.01–0.11 wt%), Mn (0.02–0.1 wt%), Cr (0.1 wt%), Mg (0.45–0.7 wt%), Zn (0.25 wt%), Ti (0.15 wt%)
AZ31 Mg alloy	Mg (Bal.), Al (3–3.2 wt%), Zn (0.8 wt%), Mn (0.4 wt%)

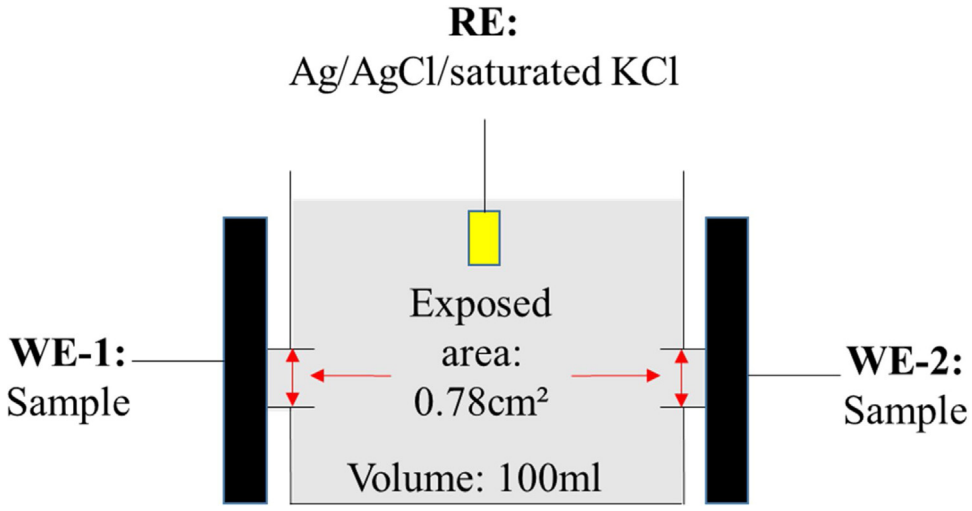

Fig. 1 – Schematic illustration of the setup for galvanic current measurement.

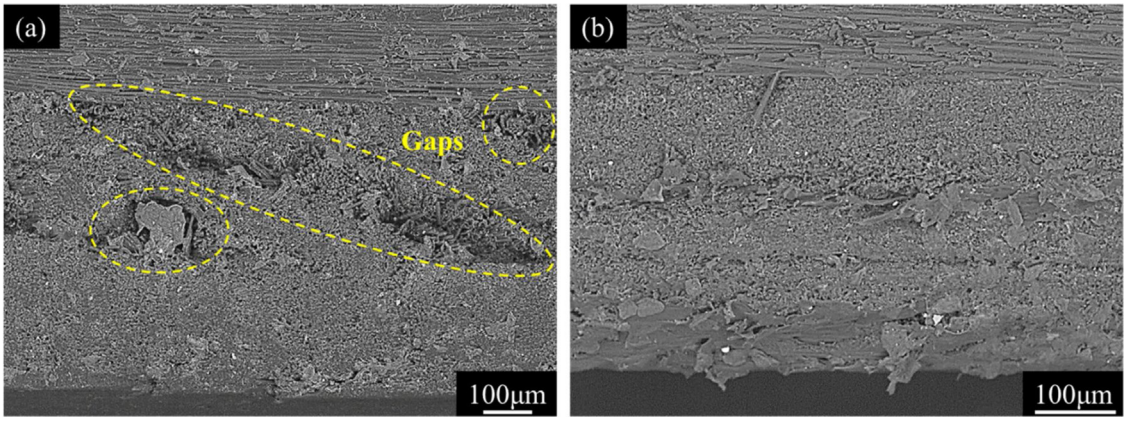

Fig. 2 – Cross-section morphologies of (a) E-CFRP and (b) T-CFRP.

platinum [28]. In practice, there are five basic factors that can influence the galvanic corrosion: (1) the potential difference between the anode and cathode, (2) the anodic polarization resistance of the anode, (3) the cathodic polarization resistance of the cathode, (4) the solution resistance between the anode and cathode, and (5) the area ratio of the cathode to anode [29,30]. In this study, the OCP differences between the CFRPs and metals were all significantly larger than 50 mV, indicating that the galvanic corrosion could be severe when the CFRPs were coupled with those metals. According to the OCP measurements, the OCP order of the samples from positive to negative was: T-CFRP > E-CFRP > 1040-steel > 6022-Al alloy > Zn coated DP590-steel > AZ31-Mg alloy. All the materials reached their relatively stable OCP values rapidly except the E-CFRP which fluctuated and took about 1.5 h to become stable.

3.3. *Potentiodynamic polarization curves*

Fig. 4 shows the potentiodynamic polarization curves of all the test samples and the intersections between the curves

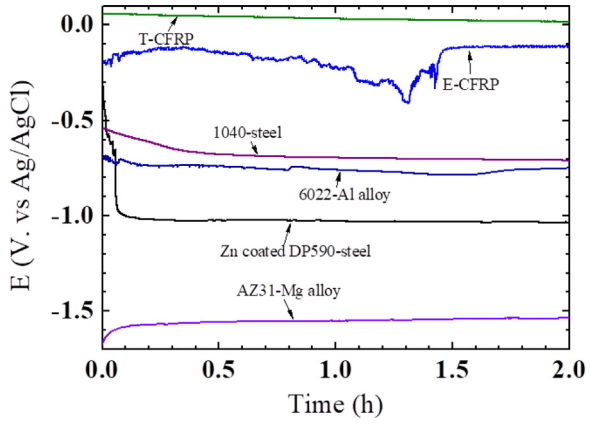

Fig. 3 – Open circuit potentials of AZ31 Mg, DP590 steel, 1040 steel, Al 6022, T-CFRP and E-CFRP.

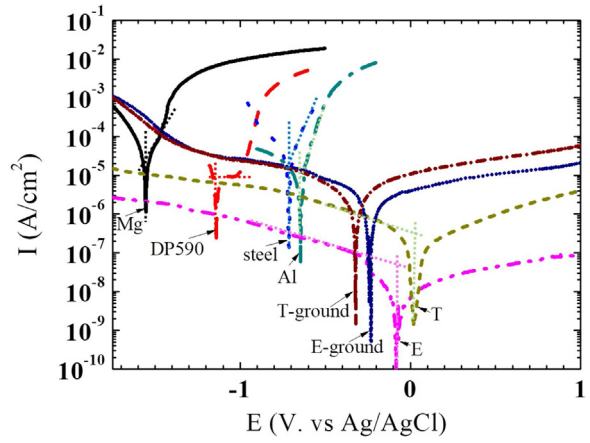

Fig. 4 – Potentiodynamic polarization curves of AZ31 Mg, DP590 steel, 1040 steel, Al 6022, T-CFRP, E-CFRP, T-CFRP-ground and E-CFRP-ground.

of the CFRPs and metals. In the CFRPs/metal couple systems, the CFRPs were cathodes and the metals were anodes. The galvanic systems were cathodic reaction/oxygen diffusion controlled, and their overall galvanic reaction rates were limited by the diffusion processes on the CFRP surfaces.

3.4. *AC-impendence*

Fig. 5 shows the EIS spectra of the CFRPs at their OCPs changing with immersion time. In experiment, the repeatability of E-CFRP was much worse than T-CFRP. Nevertheless, the resistance of E-CFRP was significantly higher than T-CFRP by a few order of magnitude [27]. The most important observation was that the EIS spectra of the E-CFRP and T-CFRP varied differently with immersion time. The E-CFRP behaved like an organic coating on metals [31,32]; its impedance at low frequencies decreased with immersion time from $10^9\ \Omega\,cm^2$ to $10^4\ \Omega\,cm^2$. However, the low frequency impedance of the T-CFRP decreased in the first 2 h and then quickly reached a stable value around $10^5\ \Omega\,cm^2$. Another interesting characteristic of the measured EIS spectra of the T-CFRP was the appearance of Warburg impedance in the low frequency range all the time, indicating that the electrochemical process on the T-CFRP after immersion in the solution was diffusion controlled. The EIS spectra of these CFRPs at −1 V have been reported before [8] and are not presented in this paper.

For comparison, the EIS measurements under the same conditions were also carried out on ground surfaces of the CFRPs. Fig. 6 shows the variation of their EIS spectra with immersion time at OCP and −1 V/Ag/AgCl. Their EIS spectra were very stable at the OCPs in the whole test time, the estimated impedance values were about $10^4\ \Omega\,cm^2$, and the T-CFRP had impedance slightly lower than the E-CFRP. When a polarization voltage of −1 V (vs OCP) was applied to the ground CFRPs, their low frequency impedances increased initially and then quickly became stable. This was probably caused by the generation of gas bubbles in the effective pores in the CFRP surface polymer layers and the damage of the polymer surfaces to some degree in the beginning [27]. This effect disappeared quickly after the polymer surfaces were completely wetted. Overall, the impedances of the ground CFRPs changed insignificantly with time (Fig. 6) compared with those of the CFRPs with their original surface polymer layers before grinding (Fig. 5).

The EIS spectra of the metals changed with immersion time at OCP are shown in Fig. 7. Considering for the complicated EIS behaviour of metals, the low frequency impedances (0.1 Hz) were simply used to represent R_p. Compare with the EIS spectra of the CFRPs, the impedances of the metals were much lower.

3.5. *Galvanic current density*

The experimentally measured galvanic current densities of all the CFRP/metal couples are shown in Fig. 8. The E-CFRP/metal couples had lower galvanic current densities than those of the T-CFRP/metal couples initially, which corresponded well to the intersection points of their potentiodynamic polarization curves. For all the T-CFRP/metal couples, the galvanic current densities started from relatively high values, but rapidly decreased with time and eventually reached relatively low stable levels. On the contrary, the galvanic current densities of the E-CFRP/metal couples were initially low, but they increased with time, and finally became higher than those of the T-CFRP/metal couples. In addition, it took a longer time for the E-CFRP/metal couples than the T-CFRP/metal couples to reach a relatively steady galvanic current density. Although the galvanic current densities of the E-CFRP/1040-steel and the T-CFRP/1040-steel couples did not intercross within the testing time in Fig. 8c, they had clearly shown an intercrossing trend.

According to these curves, the galvanic corrosion damage of the couples can be compared, which are listed in Table 2. When the E-CFRP was coupled with different metals, its galvanic current densities could be arranged in a decreasing order: AZ31-Mg alloy > Zn coated DP590 > 1040-steel > 6022-Al alloy. If the T-CFRP was coupled with the metals, then the galvanic current densities would have a following decreasing order: 1040-steel > AZ31-Mg alloy ≈ Zn coated DP590 > 6022-Al alloy. In fact, the differences in galvanic current density among the T-CFRP/metal couples were not very significant. The same

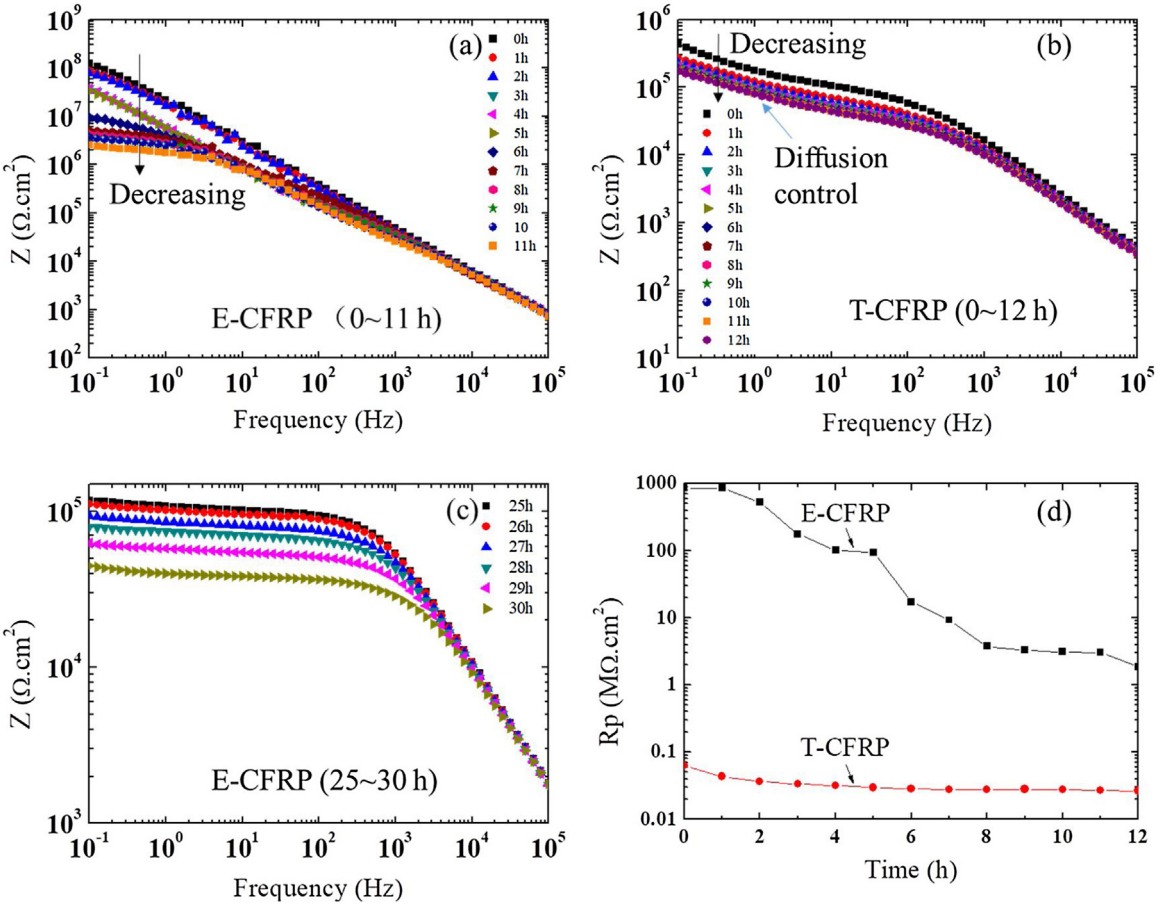

Fig. 5 – EIS spectra at different immersion times at the OCPs for: (a) E-CFRP (not ground) during 0–12 h, (b) T-CFRP (not ground) during 0–12 h, (c) E-CFRP (not ground) during 25–30 h, and (d) the changes of the estimated R_ps with immersion time for the unground E-CFRP and T-CFRP.

Table 2 – Measured galvanic current densities of CFRP/metal couples.

	E-CFRP (initially) (μA/cm²)	E-CFRP (8 h) (μA/cm²)	T-CFRP (initially) (μA/cm²)	T-CFRP (8 h) (μA/cm²)
AZ31-Mg	2.9	9.7	6.9	3.7
DP590	1.9	6.1	6.8	3.5
1040-steel	1.1	4.2	5.8	4.7
6022-Al	0.3	2.3	1.0	0.8

result has been predicted by the potentiodynamic polarization curves (see Fig. 4).

Fig. 9 presents a comparison in galvanic current density between E-CFRP/Zn coated DP590 and T-CFRP/Zn coated DP590 couples after the surface polymer layers of the CFRPs were removed by grinding. It shows that: (1) the galvanic current densities became much higher after the CFRP surface were ground, (2) the difference between the galvanic current densities of the E-CFRP/Zn coated DP590 and T-CFRP/Zn coated DP590 became much smaller after the CFRP surfaces were ground, and (3) the couples with ground CFRPs reached a steady state much more quickly.

3.6. *Overall corrosion damage*

After galvanic current measurements, the CFRP and metal surfaces were examined, and their surface morphologies are presented in Figs. 10 and 11. The DP590 coupled with E-CFRP was slightly more seriously corroded than that with T-CFRP after the first week. The difference became more obvious with duration time. After 4 weeks of testing, there was a large amount of red rust (i.e., the Zn coating had been completed dissolved and the substrate Fe was corroded) on the surface of DP590 coupled with E-CFRP. On DP590 coupled with T-CFRP, only some white rusts could be observed throughout the test time, indicating that the Zn coating was still there, not penetrated by corrosion attack. The morphologies of CFRPs after the galvanic current measurements did not change except the appearance of a mechanical mark in the area where had been sealed by a rubber ring during the test (see Fig. 11). This suggests that the CFRPs simply acted as cathodes and themselves were not significantly affected by the metal.

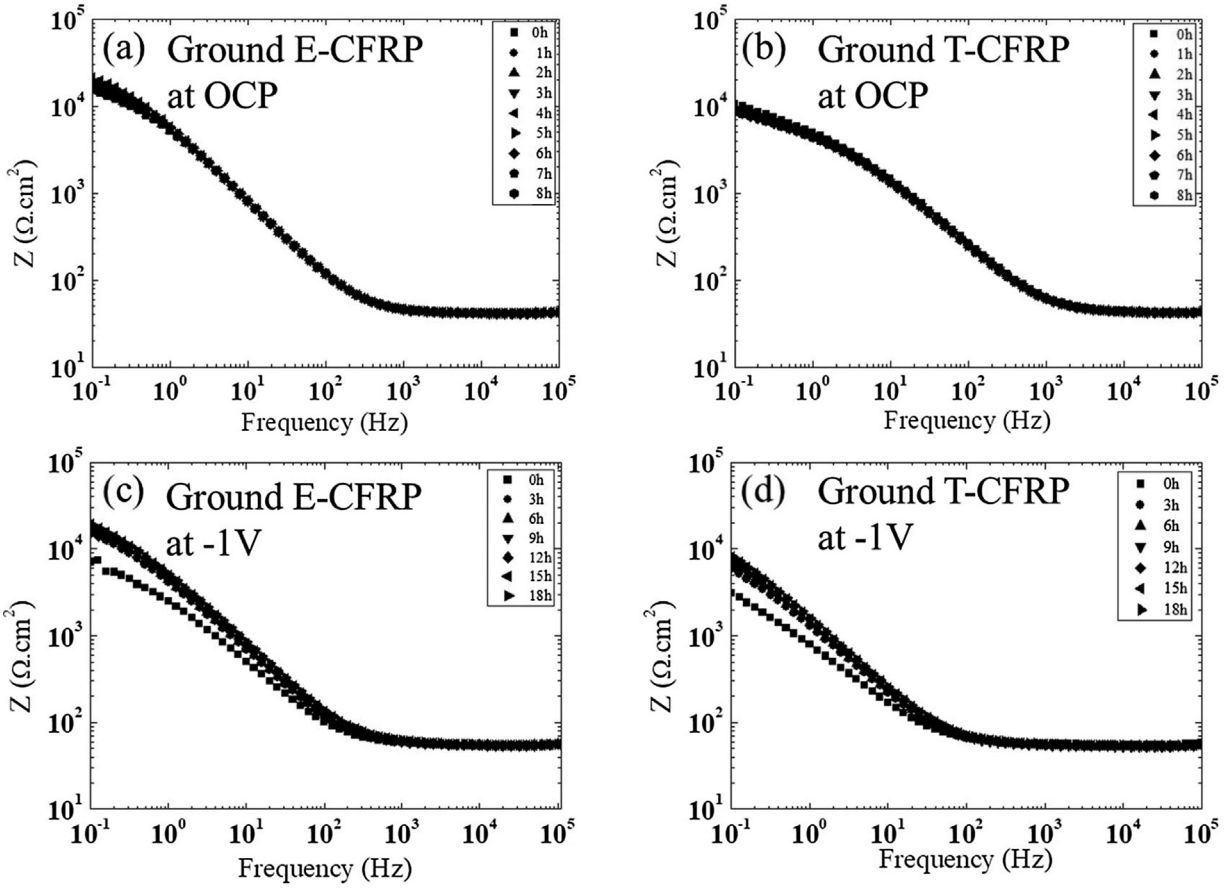

Fig. 6 – EIS spectra at different immersion times for: (a) ground E-CFRP at OCP, (b) ground T-CFRP at OCP, (c) ground E-CFRP at −1 V, and (d) ground T-CFRP at −1 V.

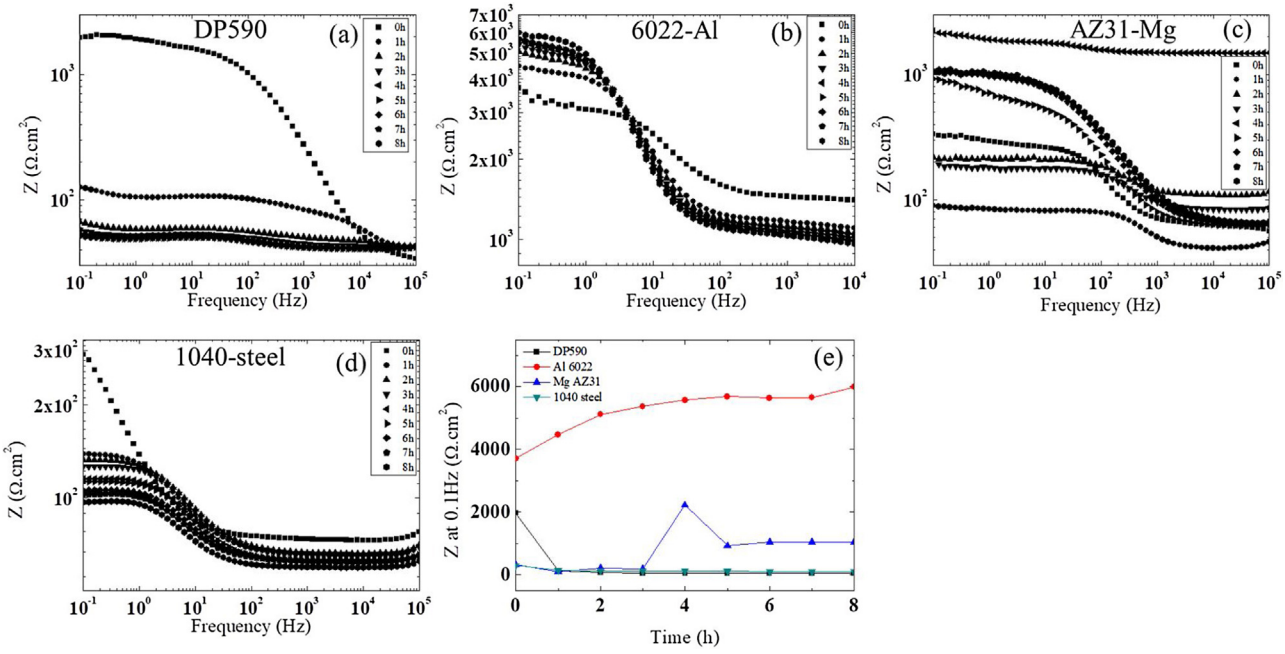

Fig. 7 – The EIS spectra at different immersion times for: (a) DP590, (b) 6022-Al, (c) AZ31-Mg, and (d) 1040-steel at their OCPs and (e) the changes of their impedances at 0.1 Hz with time.

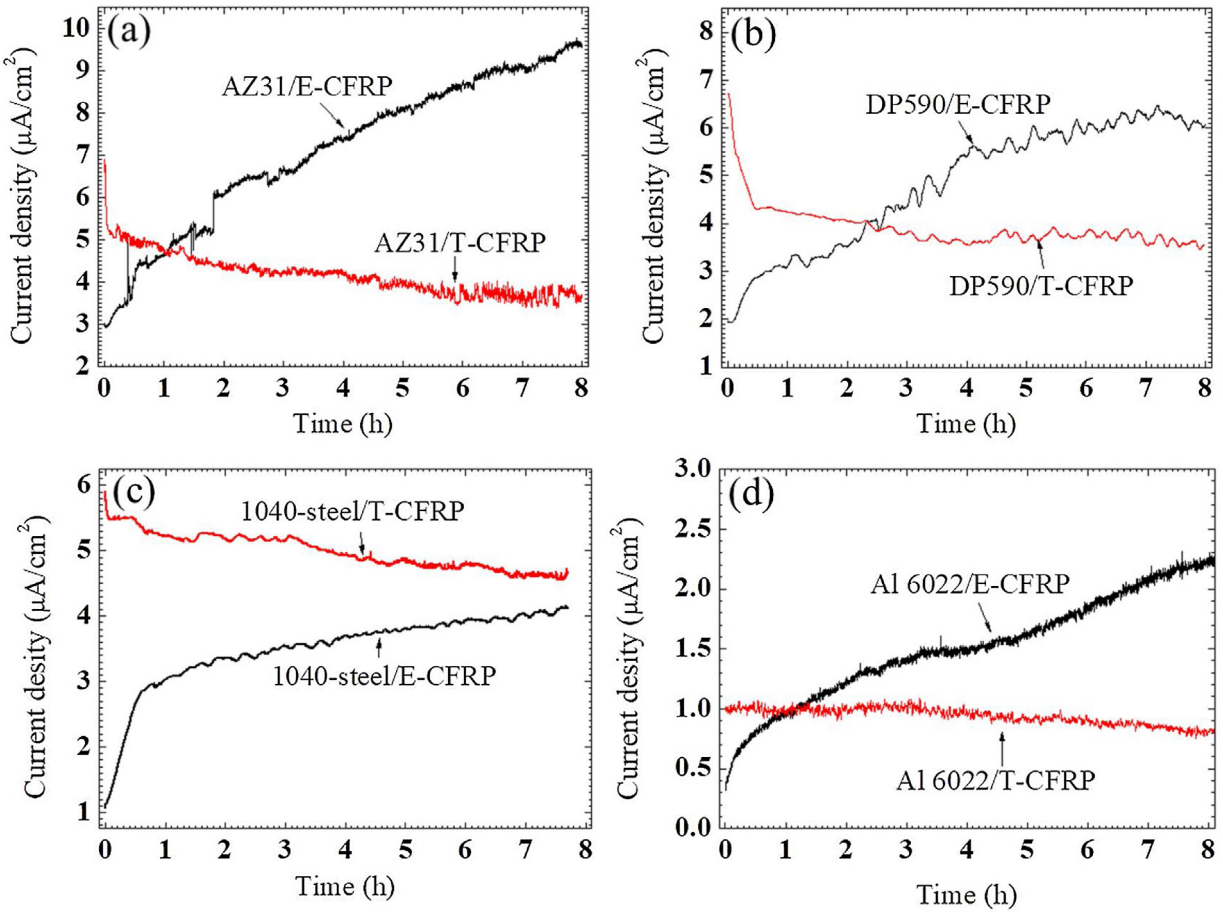

Fig. 8 – Galvanic current densities of CFRP (not ground)/metal couples: (a) CFRPs (not ground) coupled with AZ31-Mg alloy, (b) CFRPs (not ground) coupled with Zn coated DP590, (c) CFRPs (not ground) coupled with 1040-steel, and (d) CFRPs (not ground) coupled with 6022-Al alloy.

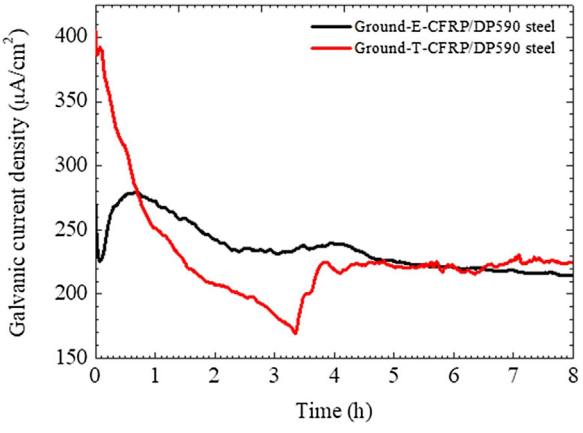

Fig. 9 – Variations of the galvanic current densities between the Zn-coated DP590 and ground CFRPs with time.

4. Discussion

According to the report by Mandel and Krüger [33], carbon fibre bundles cannot be completely embedded in a polymer, and may be exposed to the electrolyte in some areas after immersion. This idea was further developed recently in a surface polymer model, in which the exposure of carbon fibre was believed to be through "effective pores" [27]. The above results can be explained if this model is further developed to involved the ingress of corrosive species with time in the effective pores.

4.1. *Galvanic corrosion and self-corrosion*

The bulk resistivity of CFRPs is very low because they are electrically conductive [8]. Thus, the traditional galvanic theory, in which the resistance of anode and cathode is normally negligible, can be directly applied to the CFRPs/metal couples.

In this study, the corrosion potentials of the E-CFRP and T-CFRP were much more positive than the metals, thus there would be a risk of galvanic corrosion if the CFRPs and metals were joined together in a corrosive environment. The driving force for the galvanic corrosion caused by the T-CFRP was stronger than that caused by the E-CFRP, because the former's OCP was more positive than the latter's.

The galvanic corrosion rate of a couple can be predicted by the intersection between the anodic polarization curve of the anode and the cathodic polarization curve of the cathode of the system, and the self-corrosion rate of a metal

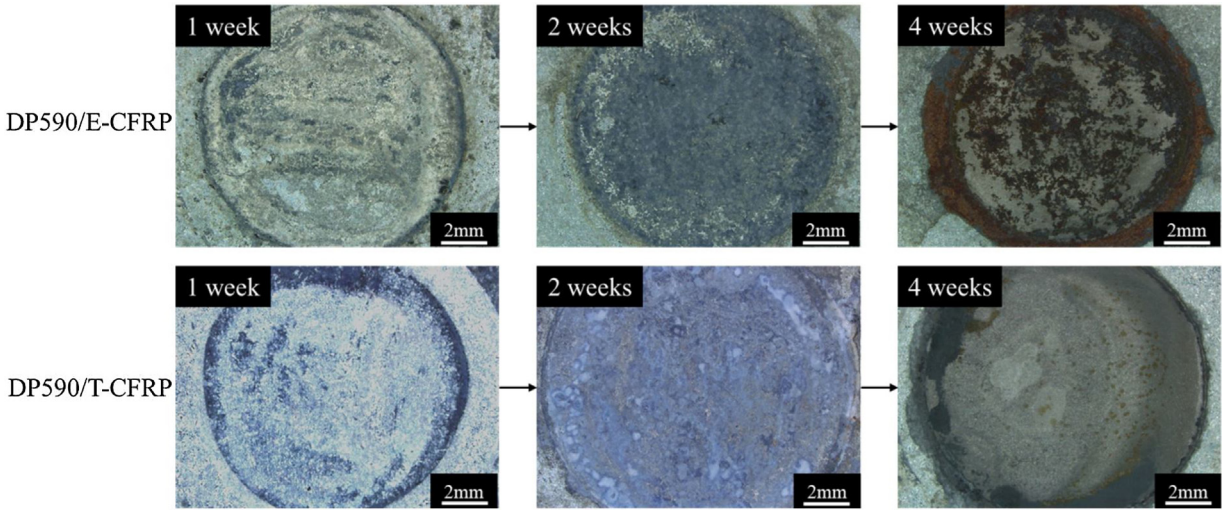

Fig. 10 – Morphologies of the corrode areas of DP590 coupled with CFRPs (not ground) changing with test time.

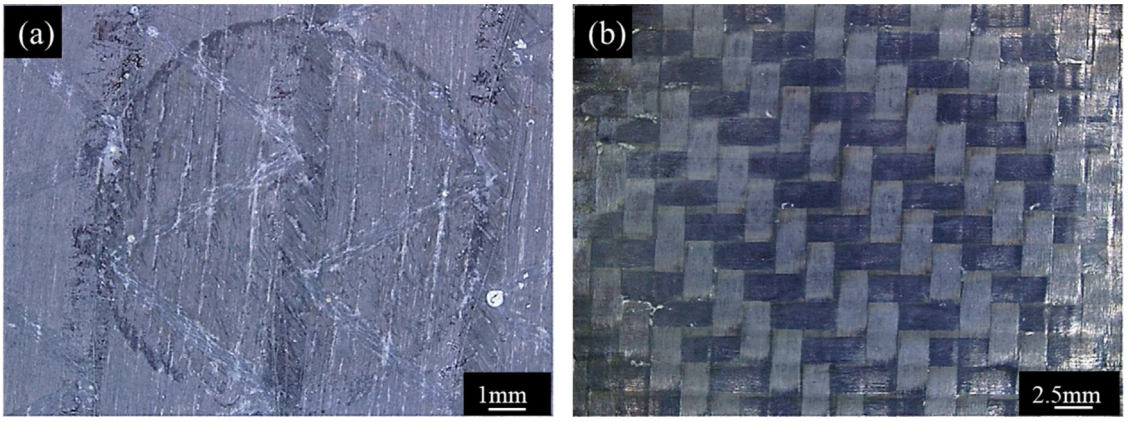

Fig. 11 – Morphologies of exposed areas of (a) E-CFRP (not ground) and (b) T-CFRP (not ground) after 4 weeks of testing.

Table 3 – Corrosion current densities and galvanic current densities of metals coupled with E-CFRP and T-CFRP before and after grinding.

	Self-corrosion rate ($\mu A/cm^2$)	I_g with E-CFRP ($\mu A/cm^2$)	I_g with T-CFRP ($\mu A/cm^2$)	I'_g with Ground-E-CFRP ($\mu A/cm^2$)	I'_g with Ground-T-CFRP ($\mu A/cm^2$)
AZ31-Mg	24.46	2.27	11.80	137.74	109.90
DP590-steel	7.14	0.97	6.64	23.39	23.12
1040-steel	14.63	0.31	3.77	14.81	14.70
6022-Al	4.45	0.27	3.13	11.58	11.49

can be estimated from its anodic and cathodic polarization curves through Tafel extrapolation. Table 3 lists the estimated self-corrosion rates (corrosion current densities, I_{corr}s) of the metals and the predicted galvanic corrosion rates (galvanic current densities, I_gs) of these metals coupled with the CFRPs before and after surface grinding based on their polarization curves shown in Fig. 4. For both CFRPs with original surface polymer layers before grinding, their I_{corr}s are larger than I_gs, which means that the galvanic corrosion damage was less severe than the self-corrosion of the metals. This is understandable, as the cathodic reactions on the CFRPs were much slower than the reactions on these metals (see Fig. 4). Therefore, the self-corrosion of the metals could not be ignored when they were coupled with CFRPs. The results in Table 3 suggest that the T-CFRP is much more detrimental than the E-CFRP in terms of the galvanic effect if they are in contact with a metal, and the detrimental galvanic effect of these two CFRPs on different metals can be ranged in a decreasing order: AZ31-Mg alloy > Zn coated DP590-steel > 1040-steel > 6022-Al alloy.

After the surface polymer layers were removed by grinding all the apparent galvanic current densities I'_gs dramatically increased, but their ranging order of galvanic corrosion damage was not changed. The similarity in polarization behaviour for the E-CFRP and T-CFRP after surface grinding obviously resulted from the exposure of carbon fibre bundles to the solution. The exposed carbon fibre bundles could cause more

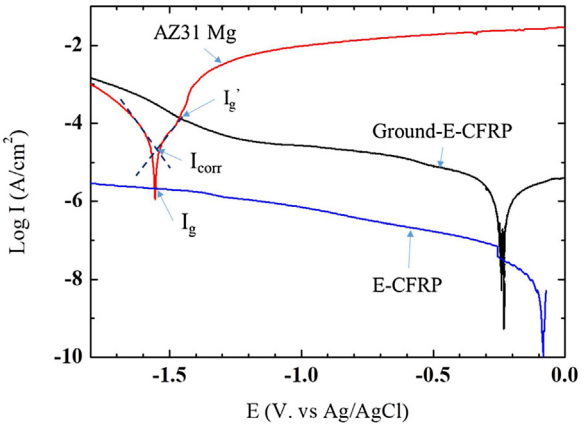

Fig. 12 – The corrosion current density (I_{corr}) of AZ31 estimated from its anodic and cathodic Tafel extrapolations and the galvanic current densities (I_gs) between AZ31 and coupled CFRPs (not ground) predicted from their polarization curves.

serious galvanic damage on the metals according to the polarization curves (see Fig. 4). In this case, the self-corrosion (I_{corr}s) may become relatively insignificant compared with the galvanic corrosion damage (I'_gs) of a coupled metal.

Fig. 12 shows typical intersections between the polarization curves of a metal (AZ31) and a CFRP (E-CFRP) before and after grinding. The self-corrosion rate I_{corr} of the metal can be estimated through Tafel extrapolation. The intersection point of the cathodic polarization curve of the CFRP and the anodic polarization curve of the metal represents the galvanic current density I_g between the metal and CFRP. It can be observed that $I_g < I_{corr} < I'_g$, indicating that galvanic corrosion was more severe in the ground-CFRP/metal couples than in the CFRP/metal couples, and the self-corrosion had an important contribution to the overall corrosion damage.

It should be noted that the E_g of the unground CFRP coupled with the metal was nearly equal to the E_{corr} of the metal. That means the galvanic current density or the dissolution rate of the metal caused by the CFRP due to galvanic effect was close to its self-corrosion rate I_{corr}. However, after the surface polymer layer was removed by grinding, the cathodic current density of the CFRP dramatically increased, and the intersection point between the polarization curves of the ground CFRP and the metal became much more positive than the E_{corr}. At this E_g, the anodic dissolution rate or galvanic current density I_g of the metal would be significantly higher than I_{corr}.

4.2. *Development of galvanic corrosion*

The most important finding in this study was the changing galvanic current densities with time as shown in Fig. 8. The galvanic currents caused by the two different CFRPs had very different changing trends, and different anode metals did not alter these differences.

Initially, the measured impedance values of the metals were a few orders of magnitude lower than those of the CFRPs (compare the impedance values in the low frequency range in Figs. 5 and 7), which are consistent with polarization curve measurements (see the extrapolation of the cathodic Tafel straight lines at the corrosion potentials of the CFRPs and the extrapolation of the anodic Tafel straight lines at the corrosion potentials of the metals in Fig. 4). In fact, the CFRPs were always much more resistant than the metals during the whole test period (Figs. 5 and 7). Therefore, the galvanic current of a CFRP/metal galvanic couple mainly depends on the cathodic polarization resistance of the CFRP, which is actually determined by the initial microstructure and thickness of the CFRP surface polymer layer. A thicker and less porous CFRP normally has a larger cathodic polarization resistance. During immersion, in addition to the microstructure and thickness, the change of the galvanic current with time is also closely associated with water ingress and corrosion product accumulation in the surface polymer layer of the CFRP. Hence, the microstructure of CFRP is a critical factor influencing the galvanic behaviour of the system.

According to Reuvers et al. [34], the development of an EIS spectra with time for a coating system can be divided into three stages: (1) a polymer film is exposed to the solution and water starts to enter the polymer, (2) the entered water reaches the metal matrix, and (3) the polymer containing a significant amount of water becomes conductive and the water fills the interface of polymer/metal. The surface polymer layer of a CFRP can be regarded as a coating on carbon fibre bundles in the study (epoxy as coating and carbon fibre as conductive matrix). Corresponding to the three stages, the CFRP surface layer will have a decreasing capacitive resistant behaviour (i.e., the resistance plateau and the following capacitance slope) firstly and then another capacitive resistant behaviour will appear (Fig. 5). The EIS results supported the different changes of the galvanic processes of the E-CFRP/metal and T-CFRP/metal couples with immersion time (Fig. 8). The E-CFRP had a much higher impedance in the low frequency range than the T-CFRP initially. However, it decreased with immersion time, while the low frequency impedance of the T-CFRP decreased and reached a relatively stable value quickly. The electrochemical process on the T-CFRP was always controlled by diffusion process (see the Warburg impedance characteristics in Fig. 5). These confirm that the electrode state changed with immersion time. In addition, T-CFRP exhibited a diffusion control process at low frequencies while E-CFRP did not (Fig. 5). It should be noted that both the CFRPs had a diffusion control process at low frequency, but the diffusion behaviour of E-CFRP could be concealed by its large resistance and thus could not be exhibited in the frequency range in the study. The diffusion-controlled processes of both the CFRPs disappeared when their surface polymer layers were removed (Fig. 6), meaning that the surface polymer layers did significantly affect the galvanic processes.

The variation of the measured EIS spectra with time for the CFRPs under −1 V/Ag/AgCl polarization [8] was similar to that of the EIS spectra at their OCPs. Their impedances in low frequencies also decreased with immersion time. The resistance of the E-CFRP gradually decreased, whereas that of the T-CFRP at the beginning decreased rapidly, but quickly stabilized at steady value. Cathodic polarization led to a more significantly decreased impedance in the low frequency range for the E-CFRP than the T-CFRP. The impedance under the cathodic polarization condition decreased faster than that at

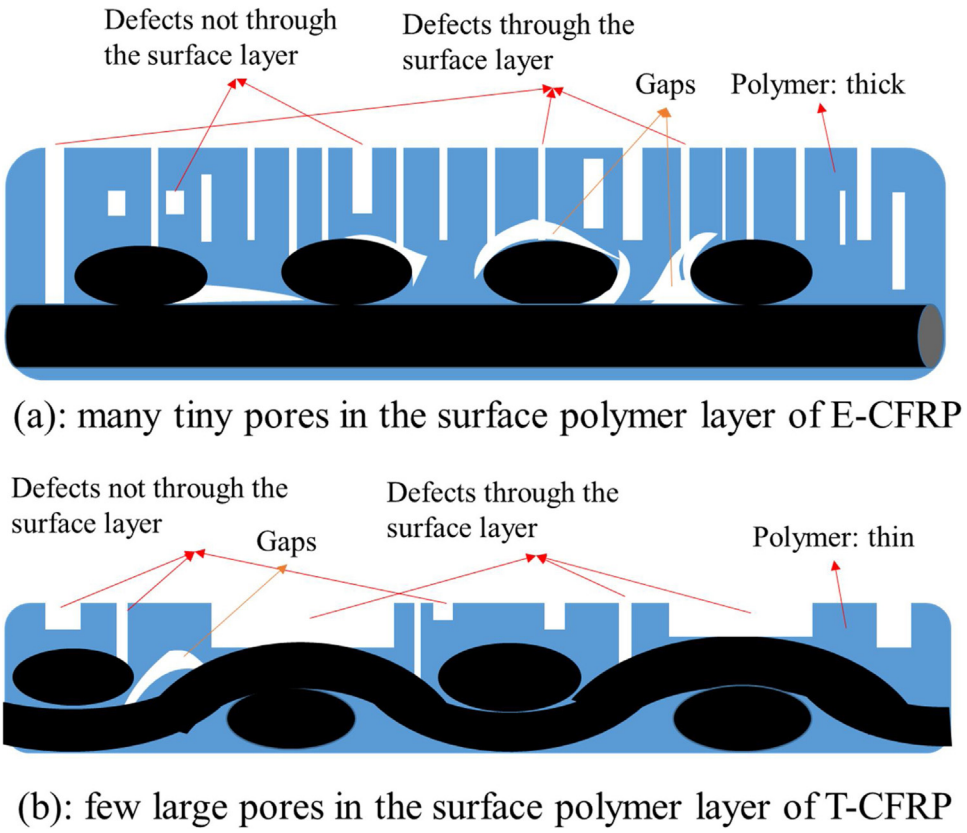

Fig. 13 – Illustration of pore-defects in the surface polymer layers of (a) E-CFRP and (b) T-CFRP.

OCP, because polarization could accelerate the water diffusion and cause damage in the surface layers of the CFRPs to some extent. The impedance of the T-CFRP becoming stable quickly implies that the cathodic polarization did not influence its surface polymer layer too much.

4.3. *Effect of the defects in surface layer*

The above changes in EIS parameters can be interpreted by a water up-take process into the surface polymer layers, which can be better understood based on the surface polymer layer model proposed recently [27] if more defect details are considered in the model, including the number and distribution of the defects in the surface polymer layer (see Fig. 13). The morphologies of defects are schematically simplified into rectangles in the model. The defects are diverse, but only the through pores, which connect the carbon fibre and the environment, can significantly affect the electrochemical behaviour of the CFRP. The through pores were denoted as "effective defects". The number of effective defects in the surface polymer layer of the E-CFRP is large and there are many gaps between carbon fibre and the polymer surface layer, but the surface polymer layer is relatively thick, while in the surface polymer layer of the T-CFRP, there are fewer effective defects and gaps, but the defects are larger.

The model has the following characteristics: (1) there are two kinds of defects: those effective pores that penetrate through the surface polymer layer from the top surface to the first layer of the carbon fibler providing shortcuts for the soultion in the environment to reach the carbon fibre, and the others that are ineffective non-through pores, having no contribution to the penetration of solution through the surface polymer layer, (2) only the effective defects exist in the surface polymer layer can significantly affect the electrochemical behaviour of a CFRP, and the contribution of those below the first layer of cabon fibre bundles is limited, (3) there are gaps between carbon fibre and polymer (Fig. 2), and (4) the environment solution penetrates larger through-pores (effective pores) preferentially, while the relatively smaller effective through-pores can also be gradually penetrated by water. Based on these, an equivalent circuit (Fig. 14) can be employed to interpret the electrochemical behaviours of the CFRPs. The circuit can be simplified into a simple one in Fig. 15 by letting $R_p = \frac{1}{\sum_{i=1}^{n} 1/R_{pi}}$, $R_c = \frac{1}{\sum_{i=1}^{n} 1/R_{ci}}$, $R_g = \frac{1}{\sum_{i=1}^{n} 1/R_{gi}}$, $\sigma_{\omega c} = \frac{1}{\sum_{i=1}^{n} 1/\sigma_{\omega ci}}$ and $\sigma_{\omega g} = \frac{1}{\sum_{i=1}^{n} 1/\sigma_{\omega gi}}$. According to the EIS results in this paper, E-CFRP and T-CFRP should have different parameter values: $R_{piE} \gg R_{piT}$, $R_{giE} \ll R_{giT} \to \infty$, n_E increased with time gradually and significantly, and n_T increased with time immediately and insignificantly. The differences in these parameters determine that the electrochemical behaviours of E-CFRP and T-CFRP are quite different. Although the parameters R_p, R_c and R_g are meaningful, they cannot be easily separated in the EIS results and spectrum-fitting for a real system (Fig. 16). Therefore, the EIS results are not fitted, and the equivalent circuits are simply used to help understand the degradation of the CFRPs in this paper.

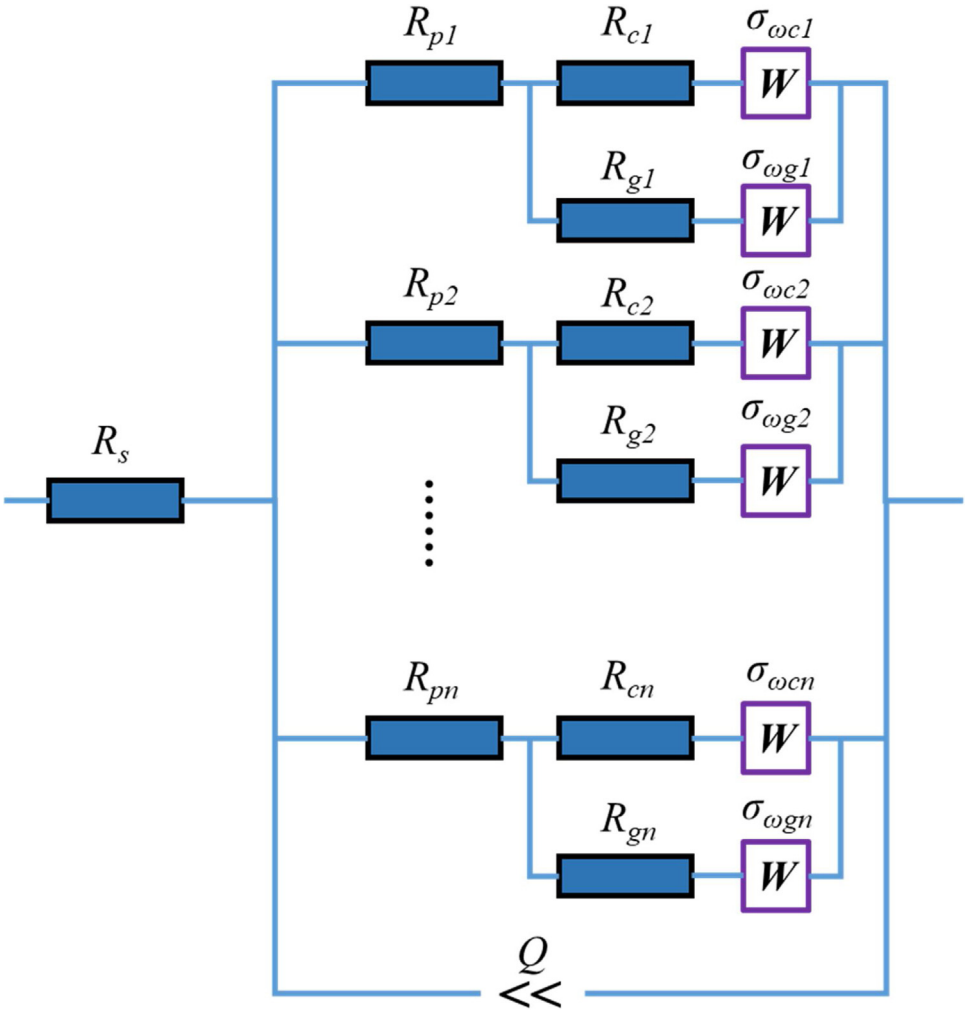

Fig. 14 – Equivalent circuit for the surface polymer layer of a CFRP in solution, in which R_p: resistance of the effective through-pores in the surface polymer layer filled with water; R_c: polarization resistance of the carbon fibre surface exposed to the water in the effective through-pores; R_g: resistance of the gaps filled with water at the interface between the surface polymer layer and carbon fibre; $\sigma_{\omega c}$: Warburg resistance on the carbon fibre surface exposed to the water in the effective through-pores; $\sigma_{\omega g}$: Warburg resistance on the carbon fibre surface exposed to the water in gaps between the carbon fibre and the surface polymer layer; n: number of effective through-pores in the surface polymer layer.

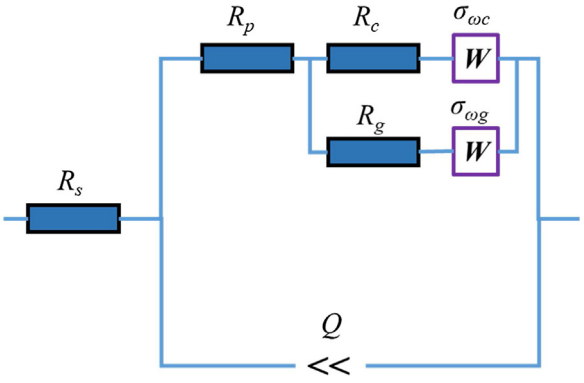

Fig. 15 – Simplified equivalent circuit of a CFRP in solution.

For E-CFRP at beginning, $R_g^0 \to \infty$, $\sigma_{\omega g}^0 \to \infty$, $R_p^0 + R_c^0 \gg \sigma_{\omega c}^0$, and thus the circuit can be further simplified into Fig. 16a, which is a typical Randles circuit and will show a semicircle spectra on the Nyqist plane or two plateaus and $a \sim -1$ slope between them on the Bode plane. Later, as $R_p^0 \to R'_p$, $R_c^0 \to R'_c$, $R_g^0 \to R'_g$, $\sigma_{\omega c}^0 \to \sigma'_{\omega c}$, $\sigma_{\omega g}^0 \to \sigma'_{\omega g}$, $Q^0 \to Q'$, $R'_c \gg R'_g$, $\sigma'_{\omega c} \gg \sigma'_{\omega g}$, $R'_p \gg R'_g$, $R'_p \gg \sigma'_{\omega g}$, $R'_g \ll R_g^0$, $R'_p < R_p^0$, and $\sigma'_{\omega g} \ll \sigma_{\omega g}^0$, the Randles circuit will have smaller resistances, and thus a smaller semicircule and lower plateaus will appear in the Nyquist and Bode plots (see Fig. 16b).

The T-CFRP is very different from E-CFRP in these parameters. For T-CFRP at beginning: $R_g^0 \to \infty$, $\sigma_{\omega g}^0 \to \infty$, $R_p^0 + R_c^0 \ll \infty$, $\sigma_{\omega c}^0 \ll \infty$, $R_p^0 + R_c^0 \sim \sigma_{\omega c}^0$. In this case, the equivalennt circuit will chang into one containing a Warburg impedance (see Fig. 16c). Hence, on the Nyquist plane, there will be a diffusion controlled impedance tail in the low frequency range in additon to the semicircle loop at high frequencies. On the Bode plane, there will be $a \sim -1/2$ slope at frequencies

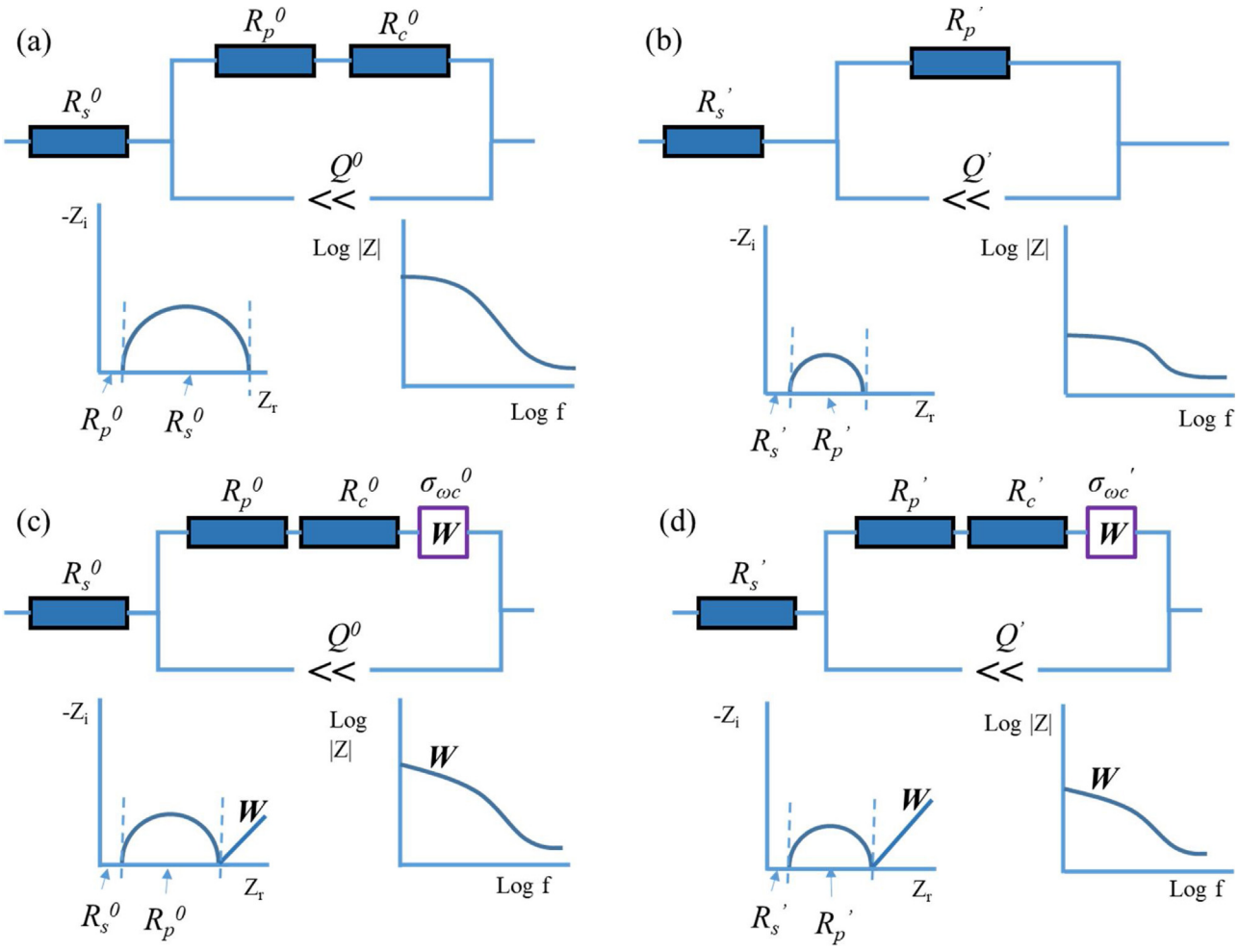

Fig. 16 – Circuits for the CFRPs: (a) E-CFRP at beginning, (b) E-CFRP later, (c) T-CFRP at beginning, and (d) T-CFRP later.

left to the R_p plateau. Quick after that, $R_p^0 \to R'_p$, $R_c^0 \to R'_c$, $R_g^0 \to R'_g \to \infty$, $\sigma_{\omega g}^0 \to \sigma'_{\omega g} \to \infty$, $\sigma_{\omega c}^0 \to \sigma'_{\omega c}$, $Q^0 \to Q'$, $R'_p \ll \infty$, $R'_c \ll \infty$, $R'_p + R'_c \ll \infty$, $R'_p + R'_c \sim \sigma_{\omega c}^0$, and $R'_p < R_p^0$. The circuit will have much smaller parameters, and the corresponding EIS spectra have smaller semicircle in Nyquist plot and low R_p plateaus in Bode plot (see Fig. 16d).

It is interesting that the metal/T-CFRP couple had a higher galvanic current density than the metal/E-CFRP initially, but the galvanic current density of the latter exceeded that of the former gradually. The phenomenon can also be explained by the model shown in Figs. 13 and 14. Comparing to the metals, the resistance of CFRP was much higher. Therefore, the galvanic current of the CFRP/metal couple system was mainly determined by CFRP. Corresponding to the three stages of water uptake and diffusion in the surface polymer layer, the circuit would change with time. In the beginning, the resistance of this system was very high, because the water just contacted the surface of the polymer layer. After that, water penetrated into the polymer through the defects inside. For E-CFRP, the number of the "large through-pore defects" exposed to the outside solution directly was very small, i.e., less parallel R_{pi}, R_{ci}, R_{gi}, $\sigma_{\omega ci}$, $\sigma_{\omega gi}$ were involved in the circuit Fig. 14. Thus, the R_p, R_g and the impedance of the surface polymer layer were high. For T-CFRP, the number of the "large through-pore defects" exposed to the outside solution directly was large, i.e., more R_{pi}, R_{ci}, R_{gi}, $\sigma_{\omega ci}$, $\sigma_{\omega gi}$ in parallel were involved in the circuit Fig. 14. Hence, the R_p, R_g and the impedance of the suface polyer layer were small. That is the reason why the resistance of E-CFRP was significantly higher than T-CFRP. With the immersion time, more and more effective through-pore defects inside the polymer were penetrated by water, i.e., the number of the parallel R_{pi}, R_{ci}, R_{gi}, $\sigma_{\omega ci}$, $\sigma_{\omega gi}$ increased, and the R_p, R_g and the impedance of the suface polyer layer decreased. In T-CFRP, the number of gaps at the carbon fibre surface was very limited. The R_p, R_g and the impedance of the suface polyer layer would not decrease further. On the contrary, there were many gaps at the polymer/carbon fibre interface in E-CFRP, i.e., the number of parallel R_{gi} was large. When water reached the inner of the surface polymer layer, the resistance would further decrease. Therefore, E-CFRP still exhibited a decreasing impedance trend, and eventually, the resistance of E-CFRP could even become lower than that of theT-CFRP. In the last stage after the the polymer was saturated by water and surface of carbon fibre under the surface polymer had been to the greatest degree exposed to water, both the CFRPs would have stable electrochemical performance. As the E-CFRP has a thicker surface polymer layer, the metal/E-CFRP took a longer time to have a relatively stable galvanic current density than

the metal/T-CFRP. As to the galvanic current densities of the metal/T-CFRP systems decreasing with immersion time, the polarization of the carbon fibre under the surface polymer layer might need to be considered. Fig. 6 indicates that the polarization resistance of the carbon fibre is around $10^4\ \Omega\,cm^2$, a few orders of magnitude smaller than that of the E-CFRP, but only one order lower than that of the T-CFRP. Thus, the polarization resistance of the carbon fibre in the E-CFRP system is negligible, but its influence on the galvanic current densities to the TCFRP cannot be ignored, particularly when the carbon fibre is cathodically polarized by the coupled metals. Fig. 6 clearly shows that the polarization resistance of the carbon fibre slightly increases after polarization at −1 V. This means that the polarization resistance of the carbon fibre in the T-CFRP could gradually increase as the surface polymer layer of the T-CFRP became less resistant, resulting in decreasing galvanic current densities of the T-CFRP/Metal systems with immersion time.

4.4. *Corrosion behaviour in practice*

The real corrosion damage is a sum of self-corrosion and galvanic corrosion. According to the galvanic current density curves shown in Fig. 8, the galvanic corrosion damage on the metals can be estimated. For example, the galvanic current density for E-CFRP/DP590 was 1.9 $\mu A/cm^2$ while T-CFRP/DP590 was 6.7 $\mu A/cm^2$ initially. The two couples reached the same galvanic current density 3.9 $\mu A/cm^2$ after 2.6 h. This means that the galvanic corrosion rate of DP590 steel in E-CFRP/DP590 couple kept increasing while in T-CFRP/DP590 couple kept decreasing. The galvanic corrosion damage caused by T-CFRP was more serious than that caused by E-CFRP. In 2.6–4.6 h, the galvanic current caused by E-CFRP became more serious than that caused by T-CFRP, and the difference became more evident with time. The integral of the galvanic current over time from 0 to 4.6 h caused by T-CFRP can be calculated to be similar to that caused by E-CFRP. After 4.6 h, the damage occurred on the DP590 caused by E-CFRP was more serious than that caused by T-CFRP. Since the damage occurred on the DP590 was an accumulated result over the whole testing period, the final damage degree should not be simply predicted by the initial or final galvanic current density.

It was noted that the different changing trends of the galvanic corrosion of the DP590 caused by the two kinds of CFRP cannot be observed from the surface morphologies after 8 h of test. According to the polarization results (see Fig. 4 and Table 2) and the above discussion, initially, the self-corrosion of the DP590 was actually even faster, causing more severe damage on the DP590 surface than the galvanic corrosion. Therefore, the slightly different galvanic corrosion caused by E-CFRP and T-CFRP could not lead to an evident difference in surface corrosion morphology in a short period time. However, with time, due to the accumulation of corrosion products on the metal surface, the self-corrosion of the metal usually could slow down, while the galvanic effect could become stronger as the resistance of the surface polymer layer could decrease by water penetration. Therefore, the contribution of the galvanic corrosion to the overall damage might become dominating compared with the self-corrosion. This was supported by the 4weeks galvanic corrosion measurement as shown in Fig. 10. According to Fig. 8b, the galvanic corrosion of DP590 caused by E-CFRP was more server than that caused by T-CFRP very quickly after a few hours of coupling in the solution. However, due to the interference of the self-corrosion, the more serious galvanic corrosion damage was clearly displayed by the surface morphology in 4 weeks (see Fig. 10).

Actually, many factors that can affect the corrosion damage in practical applications in addition to the galvanic corrosion. For example, in a galvanic couple joint, infiltration of electrolyte into the crevice between anode and cathode may also occur through capillary effect or by diffusion [35]. This is particularly likely in the crevice of a joint. Hence, crevice corrosion could not be overlooked. It is important to distinguish the contributions of galvanic corrosion, crevice corrosion and self-corrosion to the overall damage in practice.

5. Conclusions

(1) CFRPs perform similar to a noble metal with an OCP (or electrode potential) more positive than a typical engineering metal. They can cause galvanic corrosion to engineering metal in an aggressive environment.
(2) If coupled with a CFRP, the galvanic corrosion risk of different metals can be ranged in the following decreasing order: AZ31-Mg alloy > Zn coated DP590-steel > 6022-Al alloy > 1040-steel.
(3) The galvanic current density of a CFRP/metal couple is mainly determined by the surface polymer layer of the CFRP, whose resistance is much higher than that of the coupled metal. The electrochemical polarization and the galvanic behaviour are affected by water uptake and penetration in the surface polymer layer of the CFRP. Therefore, the galvanic corrosion behaviour of a CFRP/metal couples can vary significantly with time after the surface polymer layer is affected by water penetration.
(4) The T-CFRP is initially more galvanically corrosive to the metal than the E-CFRP, because the latter has a thicker and less-porous surface polymer layer with more gaps at the interface of carbon fibre and the layer than the former. However, after water penetration in to the surface polymer layers through the defects and reaching the interface gaps, the latter is more significantly affected, becoming less resistant and more galvanically corrosive.
(5) Self-corrosion has an important contribution to the overall corrosion damage of the studied engineering metals (AZ31-Mg alloy, Zn coated DP590-steel, 6022-Al alloy and 1040-steel) coupled with a CFRP. The overall corrosion behaviour of a CFRP/metal couple in a practical application can be much more complicated than the expectation by continuous galvanic current and instantaneous self-corrosion rate measurements.

Conflicts of interest

The authors declare no conflict of interest.

Acknowledgement

This work was supported by GM R&D Centre, Warren, MI, USA.

REFERENCES

[1] Ben G, Sugimoto N, Aoki Y. Development of simulation technology for impact behavior of CFRP/Al alloy hybrid beams in side collision of automobiles. Adv Comp Mater 2010;19(4):363–79.
[2] Elchalakani M. CFRP strengthening and rehabilitation of degraded steel welded RHS beams under combined bending and bearing. Thin-Walled Struct 2014;77(4):86–108.
[3] Jumaat MZ, Rahman MM, Alam MA. Flexural strengthening of RC continuous T beam using CFRP laminate: a review. Int J Phys Sci 2010;5(6):619–25.
[4] Khalifa A, Nanni A. Rehabilitation of rectangular simply supported RC beams with shear deficiencies using CFRP composites. Constr Build Mater 2002;16(3):135–46.
[5] Schnerch D, Dawood M, Sumner EA, Rizkalla S. Strengthening steel-concrete composite bridges with high modulus carbon fiber reinforced polymer (CFRP) laminates. In: Composites in construction 2005 – Third international conference. 2005.
[6] Sharples T. Applications of carbon-fiber composites to military aircraft structures. Aeronaut J 1980;84(834):177–82.
[7] Soutis C. Fibre reinforced composites in aircraft construction. Prog Aerosp Sci 2005;41(2):143–51.
[8] Zhang C, Zheng DJ, Song GL. Galvanic effect between galvanized steel and carbon fiber reinforced polymers. Acta Metall Sin 2017;30(4):342–51.
[9] Pan Y, Wu G, Cheng X, Zhang Z, Li M, Ji S, et al. Galvanic corrosion behaviour of carbon fibre reinforced polymer/magnesium alloys coupling. Corros Sci 2015;98:672–7.
[10] Peng Z, Nie X. Galvanic corrosion property of contacts between carbon fiber cloth materials and typical metal alloys in an aggressive environment. Surf Coat Technol 2013;215(4):85–9.
[11] Torres-Acosta ASA. Galvanic corrosion of steel in contact with carbon-polymer composites. II: experiments in concrete. J Comp Constr 2002;6(2):116–22.
[12] Wootton IA, Spainhour LK, Yazdani N. Corrosion of steel reinforcement in carbon fiber-reinforced polymer wrapped concrete cylinders. J Comp Constr 2003;7(4):339–47.
[13] Wielage B, Dorner A. Corrosion studies on aluminium reinforced with uncoated and coated carbon fibres. Compos Sci Technol 1999;59(8):1239–45.
[14] Wielage B, Dorner A, Shurer C, Kim JH. Corrosion protection of carbon fibre reinforced aluminium composite by diamond like carbon coatings. Mater Sci Technol 2000;16(3):344–8.
[15] Suzuki Y, Yamada T, Kimura T, Hagiwara A, Sotouchi H, Sato H, et al. Corrosion behavior of carbon fibers and graphitized carbon fibers in hot phosphoric acid. Electrochemistry 1999;67(3):259–63.
[16] Song G, Johannesson B, Hapugoda S, Stjohn D. Galvanic corrosion of magnesium alloy AZ91D in contact with an aluminium alloy, steel and zinc. Corros Sci 2004;46(4):955–77.
[17] Santos TFA, Vasconcelos GC, de Souza WA, Costa ML, Botelho EC. Suitability of carbon fiber-reinforced polymers as power cable cores: Galvanic corrosion and thermal stability evaluation. Mater Des 2015;65:780–8.
[18] Mandel M, Kruger L. Long-term corrosion behaviour of EN AW-6060-T6 in an aluminium/carbon-fibre reinforced polymer self-piercing rivet joint. Materialwiss Werkstofftech 2014;45(12):1123–9.
[19] Borrie D, Raman RKS, Zhao XL, Adnan N. Quantifying corrosion between carbon fibre reinforced polymers (CFRP) and steel caused by high temperature marine environments. Adv Struct Eng 2014;17:1761–70.
[20] Mueller Y, Tognini R, Mayer J, Virtanen S. Anodized titanium and stainless steel in contact with CFRP: an electrochemical approach considering galvanic corrosion. J Biomed Mater Res A 2007;82(4):936–46.
[21] Torres-Acosta AA, Sen R. Electrochemical behavior of coupled carbon fiber-reinforced polymer (CFRP) rods in concrete. J Appl Electrochem 2005;35(6):529–37.
[22] Serdechnova M, Kallip S, Ferreira MGS, Zheludkevich ML. Active self-healing coating for galvanically coupled multi-material assemblies. Electrochem Commun 2014;41(2):51–4.
[23] Qiu R, Zhang Q, Wang P, Jiang LN, Hou J, Guo WM, et al. Fabrication of slippery liquid-infused porous surface based on carbon fiber with enhanced corrosion inhibition property. Colloid Surf A Physicochem Eng Asp 2014;453:132–41.
[24] Liu Z, Curioni M, Jamshidi P, Walker A, Prengnell P, Thompson GE, et al. Electrochemical characteristics of a carbon fibre composite and the associated galvanic effects with aluminium alloys. Appl Surf Sci 2014;314(24):233–40.
[25] Miriyala S, Tucker W, Rockett T, Brown R. Degradation of carbon reinforced polymer composites under galvanic coupling conditions. AIAA J 1992;92:3036–45.
[26] Feng LU, Zhang X, Tang Z, Ming L. Galvanic corrosion behavior between carbon fiber reinforced plastic materials and aluminum alloys. J Chin Soc Corros Prot 2005;25(1):39–43.
[27] Zhang C, Zheng D, Song GL, Guo Y, Liu M, Kia H. Effect of the microstructure of carbon fiber reinforced polymer on electrochemical behavior. J Electrochem Soc 2018;165(10):C647–56.
[28] Danford MD, Higgins RH. Galvanic corrosion in (graphite/epoxy)/alloy couples. United States: NASA; 1988.
[29] Schneider M, Kremmer K, Lämmel C, Sempf K, Herrmann M. Galvanic corrosion of metal/ceramic coupling. Corros Sci 2014;80(3):191–6.
[30] Tostmann KH. Korrosion: Ursachen und Vermeidung; 2005.
[31] Song S, Song GL, Shen W, Liu M. Corrosion and electrochemical evaluation of coated magnesium alloys. Corrosion 2012;68(1):109–21.
[32] Song GL, Liu M. The effect of surface pretreatment on the corrosion performance of Electroless E-coating coated AZ31. Corros Sci 2012;62(9):61–72.
[33] Mel M, Krüger L. Electrochemical corrosion studies and pitting corrosion sensitivity of a self-pierce rivet joint of carbon fibre reinforced polymer (CFRP) – laminate and EN AW-6060-T6. Materialwiss Werkstofftech 2012;43(4):302–9.
[34] Reuvers NJW, Huinink HP, Adan OCG, Garcia SJ, Mol JMC. Water uptake in thin nylon 6 films as measured by electrochemical impedance spectroscopy and magnetic resonance imaging. Electrochim Acta 2013;94:219–28.
[35] Mandel M, Krüger L. Determination of pitting sensitivity of the aluminium alloy EN AW-6060-T6 in a carbon-fibre reinforced plastic/aluminium rivet joint by finite element simulation of the galvanic corrosion process. Corros Sci 2013;73(2):172–80.